DOI: https://doi.org/10.57233/ijsgs.v11i2.854 ISSNp: 2488-9229; ISSNe: 3027-1118

IJSGS FUGUSAU VOLXXX WEBSITE: https://fugus-ijsgs.com.ng

INTERNATIONAL JOURNAL OF SCIENCE FOR GLOBAL SUSTAINABILITY
(A PUBLICATION OF FACULTY OF SCIENCE, FEDERAL UNIVERSITY GUSAU, NIGERIA)

Transient Electro-Magneto Hydrodynamic (EMHD) Control of Hybrid Nanofluid Flow over 2D Riga Plate: Entropy Generation and Stability Analysis

Abdullahi Buhari[1], M. N. Sarki[2] and Sanusi Aminu Bawa[3]

[1] Department of Mathematics, Federal University Birnin Kebbi, Nigeria

[2,3]Department of Mathematics, Kebbi State University of Science and Technology Aliero, Nigeria

Corresponding Author's Email: Abdullahi.buhari@fubk.edu.ng

Received on: April, 2025 **Revised and Accepted on:** May, 2025 **Published on:** July, 2025

ABSTRACT

This study investigates the transient Electro-Magneto Hydrodynamic (EMHD) control of hybrid nanofluid flow over a two-dimensional Riga plate, focusing on entropy generation minimization and hydrodynamic stability analysis. The Riga plate, composed of alternating electrodes and permanent magnets, generates an exponentially decaying Lorentz force, which enhances boundary layer flow control. While previous research has primarily examined steady-state EMHD flows, this work addresses the transient behavior critical for real-world dynamic systems. The governing equations for momentum, energy, and nanoparticle concentration are derived and solved analytically using perturbation methods for steady-state conditions and Laplace transforms for transient solutions. A finite difference numerical scheme is employed to validate the results numerically, ensuring accuracy through convergence criteria. Key dimensionless parameters, including the modified Hartmann number (Z), Richardson number (λ), and suction parameter (s), are analyzed to assess their impact on flow, heat transfer, and stability. Results demonstrate that EMHD effects significantly enhance velocity profiles, while Prandtl number (Pr) variations influence thermal boundary layers. Entropy generation analysis reveals that thermal irreversibility dominates near the plate, whereas viscous and Joule heating effects prevail farther away. Stability studies confirm that strong suction (s) stabilizes the flow, suppressing perturbations. Additionally, Nusselt and Sherwood numbers increase with higher Z and s, indicating improved heat and mass transfer efficiency. This study provides critical insights into optimizing EMHD-based thermal systems by minimizing entropy generation and ensuring hydrodynamic stability. The findings have significant implications for microfluidics, nuclear cooling, and aerospace propulsion, where precise thermal management is essential.

Keywords: Hybrid nanofluid, Riga plate, Transient EMHD, Entropy generation, Stability analysis, Perturbation method.

Nomenclature

Roman Letters

Symbol	Definition	Units (SI)
a	Width of magnets and electrodes	m
Br	Brinkman number	$-$
Be	Bejan number	$-$
C	Nanoparticle concentration	kg/m^3
cp	Specific heat capacity	$J/(kg \cdot K)$
DB	Brownian diffusion coefficient	m^2/s
DT	Thermophoretic diffusion coefficient	m^2/s
g	Gravitational acceleration	m/s^2
$j0$	Applied current density	A/m^2
k	Thermal conductivity	$W/(m \cdot K)$
Le	Lewis number	$-$
$M0$	Magnetization of permanent magnets	A/m
Nb	Brownian motion parameter	$-$
Nt	Thermophoresis parameter	$-$
Nr	Nanoparticle flux parameter	$-$
Ns	Entropy generation number	$-$
Pr	Prandtl number	$-$
s	Suction/injection parameter	$-$
T	Temperature	K
t	Time	s
u, v	Velocity components in x, y directions	m/s

DOI: https://doi.org/10.57233/ijsgs.v11i2.854 ISSNp: 2488-9229; ISSNe: 3027-1118
IJSGS FUGUSAU VOLXXX WEBSITE: https://fugus-ijsgs.com.ng

$V0$	Suction velocity	m/s
Z	Modified Hartmann number	$-$

Greek Letters

Symbol	Definition	Units (SI)
α	Thermal diffusivity	m^2/s
β	Volumetric thermal expansion coefficient	$1/K$
Γ	Diffusion ratio	$-$
λ	Richardson number	$-$
μ	Dynamic viscosity	$kg/(m \cdot s)$
ν	Kinematic viscosity	m^2/s
ρ	Density	kg/m^3
σ	Electrical conductivity	S/m
τ	Nanoparticle heat capacity ratio	$-$
ϕ	Nanoparticle volume fraction	$-$
θ	Dimensionless temperature	$-$

Subscripts/Superscripts

Symbol	Definition
∞	Ambient condition
w	Wall condition
f	Base fluid
p	Nanoparticle
hnf	Hybrid nanofluid
s	Steady-state
t	Transient component

1.0 INTRODUCTION

The study of hybrid nanofluid flow over a Riga plate has gained significant attention in recent years due to its potential applications in advanced thermal engineering, electromagnetic flow control, and energy systems. The Riga plate, characterized by an alternating array of electrodes and permanent magnets, generates an exponentially decaying Lorentz force, which can effectively manipulate boundary layer flows. When combined with transient Electro-Magneto Hydrodynamic (EMHD) effects, this configuration offers a promising mechanism for enhancing heat transfer and controlling fluid motion in hybrid nanofluids, a novel class of fluids engineered by dispersing multiple nanoparticles in a base fluid to improve thermophysical properties.

Recent advancements in nanotechnology and electromagnetic flow control have spurred significant interest in hybrid nanofluids due to their superior thermal properties compared to conventional fluids (Choi, 1995). These engineered fluids, which suspend multiple nanoparticles (e.g., Al_2O_3, Cu) in base fluids like water, exhibit enhanced thermal conductivity, viscosity, and electrical conductivity. Such properties make them ideal for applications in heat exchangers, electronic cooling, and renewable energy systems (Mahian *et al.*, 2019). Hussanan *et al.* (2021) numerically investigated the heat transfer characteristics of hybrid nanofluids over a stretching sheet under magnetic fields, highlighting the synergy between nanoparticle interactions and Lorentz forces. Their findings align with the present study's focus on EMHD-controlled flow, particularly in validating the finite difference method for coupled momentum and energy equations. However, the interplay between electromagnetic forces and transient thermofluidic dynamics in hybrid nanofluids remains underexplored, particularly in configurations like the Riga plate, which offers unique advantages for boundary layer manipulation. Usman *et al.* (2024) investigated the impact of MHD inclination on unsteady gaseous micro-flow past a sinusoidally moving horizontal plate in the slip flow regime. Muhammad *et al.* (2024) studied Unsteady MHD free convention isothermal vertical plate in a porous medium with radiation effect numerically. Saleh *et al.* (2024) investigated Magnetohydrodynamic (MHD) Convective Flow through a Porous Medium with Magnetic and Chemical Reaction Characteristics. Dakin-Gari *et al.* (2024) investigated effect of heat and mass transfer on unsteady MHD free convective flow of Jeffrey fluid through porous medium in the presence of heat source. Saleh *et al.* (2023) studied MHD convective flow with variable pressure and injection/suction in a porous medium.

The Riga plate, first conceptualized by Gailitis and Lielausis (1961), generates a spatially decaying Lorentz force through alternating electrodes and magnets. This setup has been widely adopted in magnetohydrodynamic (MHD) studies to suppress flow separation and enhance heat transfer (Ahmad *et al.*, 2016; Ali *et al.*, 2023). While steady-state MHD flows over Riga plates have been extensively analyzed (e.g., Khatun et al., 2021 on rotating systems), transient

DOI: https://doi.org/10.57233/ijsgs.v11i2.854 ISSNp: 2488-9229; ISSNe: 3027-1118
IJSGS FUGUSAU VOLXXX WEBSITE: https://fugus-ijsgs.com.ng

effects which are critical for industrial systems with dynamic operating conditions, and these are rarely addressed. For instance, in nuclear reactors or microfluidic pumps, sudden power fluctuations or startup/shutdown processes necessitate understanding time-dependent EMHD responses (Sheikholeslami *et al*., 2022).

Entropy generation analysis further bridges this gap by quantifying irreversible energy losses, a metric pivotal for sustainable thermal system design (Bejan, 1996). Prior studies on nanofluid entropy generation have overlooked the combined effects of transient EMHD and hybrid nanoparticles. Similarly, stability analyses often neglect the role of suction/injection (Hamza *et al*., 2022), though it is a key control parameter in industrial applications. This study fills these gaps by investigating the transient EMHD effects on hybrid nanofluid flow, entropy generation mechanisms under dynamic conditions, linear stability with suction/injection effects and Practical insights for optimizing thermal systems.

However, most studies to date (e.g., Ahmad *et al*., 2015; Ali *et al*., 2023) have focused on steady-state EMHD flows, leaving transient behavior, critical for real-world dynamic systems underexplored particularly in the context of entropy generation and hydrodynamic stability. The analysis of entropy production is crucial for optimizing energy efficiency, as it quantifies irreversible losses due to thermal gradients, viscous dissipation, and electromagnetic effects. Furthermore, a stability analysis is essential to determine the robustness of the flow regime under perturbations, ensuring practical applicability in industrial systems such as microfluidic devices, nuclear cooling, and aerospace propulsion.

Steady-state Magnetohydrodynamics MHD of hybrid nanofluid flow past a 2D Riga plate has been extensively studied. Such studies include that of Ahmad *et al.* (2016), they studied the mixed convection boundary layer flow of a nanofluid past a vertical Riga plate in the presence of strong suction, incorporating Brownian motion and thermophoresis effects. Ali *et al.* (2023) investigated the enhanced heat transfer analysis of hybrid nanofluid over a Riga plate, incorporating Lorentz forces and entropy generation. Hamza *et al.* (2022) investigated the effects of Magnetohydrodynamics (MHD) on time-dependent mixed convection flow of an exothermic fluid in a vertical channel. Khatun *et al.* (2021) investigated the EMHD radiating fluid flow along a vertical Riga plate with suction in a rotating system. They noted a substantial uprise for both the secondary velocity and primary velocity under a modified Hartmann number's rising actions. While steady-state Magnetohydrodynamics (MHD) of hybrid nanofluid flow past a 2D Riga plate has been extensively studied, significant gaps remain in the understanding of transient EMHD behavior under dynamic conditions. Existing works, such as those by Ahmad *et al.* (2016) and Ali *et al*. (2023), primarily focus on steady-state scenarios, neglecting the time-dependent effects critical for real-world applications like nuclear reactors or microfluidic systems, where sudden operational changes (e.g., startup/shutdown, power fluctuations) occur. Additionally, prior studies often overlook the combined impact of transient EMHD forces, hybrid nanoparticles, and entropy generation under dynamic suction/injection conditions. The interplay between these factors is essential for optimizing energy efficiency and stability in thermal systems remains underexplored. Furthermore, while Khatun *et al.* (2021) and Hamza *et al.* (2022) address rotational and exothermic effects, their analyses lack a comprehensive evaluation of hydrodynamic stability under transient perturbations or the role of entropy minimization in time-dependent regimes. This study bridges these gaps by investigating transient EMHD control, entropy generation mechanisms, and linear stability analysis for hybrid nanofluids over Riga plates, offering novel insights for industrial applications requiring adaptive thermal management.

This study aims to investigate the transient EMHD control of hybrid nanofluid flow over a two-dimensional Riga plate, with a focus on entropy generation minimization and linear stability analysis. By employing a combination of numerical simulations and theoretical modeling, we seek to elucidate the interplay between electromagnetic forces, nanoparticle interactions, and transient flow dynamics. The findings are expected to provide valuable insights into optimizing EMHD-based thermal systems while mitigating energy losses through entropy-based design strategies.

2.0 PROBLEM FORMATION

We consider the electro-magnetohydrodynamics mixed convection boundary layer flow of a nanofluid with weakly conducting based fluid induced by a Riga plate placed at $y = 0$ with $x-$axis aligned vertically upward. The plate with suction velocity V_0 is moving with constant velocity in x direction in a viscous based nanofluid. The Riga plate consists of an alternating array of electrodes and permanent magnets mounted on a plane surface (see Fig.1). At the sheet the temperature T and the nanoparticle fraction ϕ take the constant values T_w and ϕ_w respectively. The ambient values of T and ϕ are given as T_∞ and ϕ_∞.

DOI: https://doi.org/10.57233/ijsgs.v11i2.854 ISSNp: 2488-9229; ISSNe: 3027-1118

IJSGS FUGUSAU VOLXXX WEBSITE: https://fugus-ijsgs.com.ng

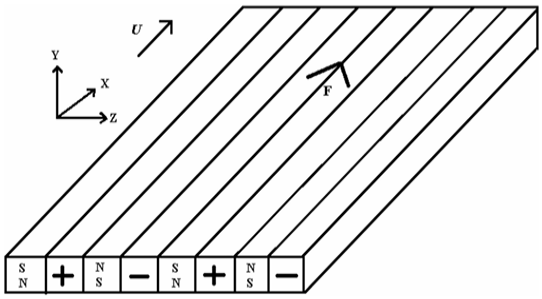

Figure 1: Schematic Diagram of Riga Plate

Employing the Oberbeck–Boussinesq approximation and the assumption that the nanoparticle concentration is dilute, the boundary layer equations for the conservation of total mass, momentum, thermal energy, and nanoparticles are written as:

$$\frac{\partial U}{\partial X}+\frac{\partial V}{\partial Y}=0 \tag{1}$$

$$\frac{\partial U}{\partial t}+U\frac{\partial U}{\partial X}+V\frac{\partial U}{\partial Y}=\frac{\mu}{\rho_f}\frac{\partial^2 U}{\partial Y^2}+(1-\phi_\infty)g\beta(T-T_\infty)-\frac{\rho_p-\rho_f}{\rho_f}g(\phi-\phi_\infty)+\frac{\pi j_0 M_0}{8\rho_f}e^{-\frac{\pi}{a}Y} \tag{2}$$

$$\frac{\partial T}{\partial t}+U\frac{\partial T}{\partial X}+V\frac{\partial T}{\partial Y}=\alpha\frac{\partial^2 T}{\partial Y^2}+\tau\left(D_B\frac{\partial T}{\partial Y}\frac{\partial C}{\partial Y}+\frac{D_T}{T_\infty}\left(\frac{\partial T}{\partial Y}\right)^2\right) \tag{3}$$

$$\frac{\partial C}{\partial t}+U\frac{\partial C}{\partial X}+V\frac{\partial C}{\partial Y}=D_B\frac{\partial^2 C}{\partial Y^2}+\frac{D_T}{T_\infty}\frac{\partial^2 T}{\partial Y^2} \tag{4}$$

Subjected to boundary conditions

$$\left.\begin{array}{llll} U=U_w, & V=V_w, & T=T_w, & C=C_w \quad at\ Y=0 \\ u\to 0, & T=T_\infty, & C=C_\infty & as\ Y\to\infty \end{array}\right\} \tag{5}$$

Introducing non-dimension variables:

$$\left.\begin{array}{lllll} x=\frac{X}{l}, & y=\frac{Y}{L}, & u=\frac{U}{U_w}, & v=\frac{V}{V_0}, & \theta=\frac{T-T_\infty}{T_w-T_\infty}, \quad \phi=\frac{C-C_\infty}{C_w-C_\infty} \\ & & L=\frac{a}{\pi}, & l=\frac{U_w L^2}{V}, & V_0=\frac{V\pi}{a} \end{array}\right\} \tag{6}$$

Substituting (6) into (1) - (4), we get:

$$\frac{\partial u}{\partial x}+\frac{\partial v}{\partial y}=0 \tag{7}$$

$$\frac{\partial u}{\partial t}+u\frac{\partial u}{\partial x}+v\frac{\partial u}{\partial y}=\frac{\partial^2 u}{\partial y^2}+\lambda\theta-Nr\phi+Ze^{-y} \tag{8}$$

$$\frac{\partial \theta}{\partial t}+u\frac{\partial \theta}{\partial x}+v\frac{\partial \theta}{\partial y}=\frac{1}{Pr}\frac{\partial^2 \theta}{\partial y^2}+Nb\frac{\partial \theta}{\partial y}\frac{\partial \phi}{\partial y}+Nt\left(\frac{\partial \theta}{\partial y}\right)^2 \tag{9}$$

$$\frac{\partial \phi}{\partial t}+u\frac{\partial \phi}{\partial x}+v\frac{\partial \phi}{\partial y}=\frac{1}{Le}\frac{\partial^2 \phi}{\partial y^2}+\frac{1}{Le}\frac{Nt}{Nb}\frac{\partial^2 \theta}{\partial y^2} \tag{10}$$

With assumption of strong suction/injection, the equations above can be reduced to:

$$\frac{\partial u}{\partial t}+v_w\frac{\partial u}{\partial y}=\frac{\partial^2 u}{\partial y^2}+\lambda\theta-Nr\phi+Ze^{-y} \tag{11}$$

$$\frac{\partial \theta}{\partial t}+v_w\frac{\partial \theta}{\partial y}=\frac{1}{Pr}\frac{\partial^2 \theta}{\partial y^2}+Nb\frac{\partial \theta}{\partial y}\frac{\partial \phi}{\partial y}+Nt\left(\frac{\partial \theta}{\partial y}\right)^2 \tag{12}$$

$$\frac{\partial \phi}{\partial t}+v_w\frac{\partial \phi}{\partial y}=\frac{1}{Le}\frac{\partial^2 \phi}{\partial y^2}+\frac{1}{Le}\frac{Nt}{Nb}\frac{\partial^2 \theta}{\partial y^2} \tag{13}$$

Subjected to boundary conditions

$$\left.\begin{array}{llll} u=1, & v=v_w, & \theta=1, & \phi=1 \quad at\ y=0 \\ u\to 0, & \theta=0, & \phi=0 & as\ y\to\infty \end{array}\right\} \tag{14}$$

The dimensionless parameters in the equations above are defined by:

$$\left.\begin{array}{llll} \lambda=\frac{a^2\Delta T}{\pi^2 v U_w}(1-\phi_\infty)g\beta, & Z=\frac{a^2 j_0 M_0}{8\pi v U_w \rho_f}, & Nr=\frac{a^2\Delta\phi}{\pi^2 v U_w}\left(\frac{\rho_p-\rho_f}{\rho_f}\right)g, & \\ Nt=\frac{\tau D_T \Delta T}{v T_\infty}, & Nb=\frac{\tau D_B \Delta C}{v}, & v=\frac{\mu}{\rho_f}, & Pr=\frac{v}{\alpha}, \quad Le=\frac{v}{D_B} \end{array}\right\} \tag{15}$$

2.1 Physical Properties of Hybrid Nanofluid

The following are the thermo-physical properties of hybrid nanofluids:

DOI: https://doi.org/10.57233/ijsgs.v11i2.854 ISSNp: 2488-9229; ISSNe: 3027-1118
IJSGS FUGUSAU VOLXXX WEBSITE: https://fugus-ijsgs.com.ng

2.1.1 Density (ρ)

$$\rho_{hnf} = (1-\phi_1-\phi_2)\rho_f + \phi_1\rho_{p1} + \phi_2\rho_{p2} \quad (16)$$

where ρ_f, ρ_{p1} and ρ_{p2} are densities of water, aluminum oxide and copper respectively.

2.1.2 Heat Capacity

$$(\rho c_p)_{hnf} = (1-\phi_1-\phi_2)(\rho c_p)_f + \phi_1(\rho c_p)_{p1} + \phi_2(\rho c_p)_{p2} \quad (17)$$

2.1.3 Thermal Conductivity

Using Maxwell-Garnetts model for spherical nanoparticles

$$\frac{k_{hnf}}{k_f} = \frac{\left(k_{p1}+2k_f-2\phi_1(k_f-k_{p1})\right)\left(k_{p2}+2k_f-2\phi_2(k_f-k_{p2})\right)}{\left(k_{p1}+2k_f-\phi_1(k_f-k_{p1})\right)\left(k_{p2}+2k_f-\phi_2(k_f-k_{p2})\right)} \quad (18)$$

2.1.4 Dynamic Viscosity

By Brinkman model

$$\mu_{hnf} = \frac{\mu_f}{(1-\phi_1-\phi_2)^{2.5}} \quad (19)$$

2.1.5 Electrical Conductivity

$$\frac{\sigma_{hnf}}{\sigma_f} = \frac{3\left(\phi_1(\sigma_{p1}-\sigma_f)+\phi_2(\sigma_{p2}-\sigma_f)\right)}{(\sigma_{p1}+2\sigma_f)-(\phi_1+\phi_2)(\sigma_{p1}+\sigma_{p2}-2\sigma_f)} \quad (20)$$

Table 1: Numerical Values of Base Fluid and Nanoparticles Thermo-Physical Characteristics

Physical Properties	Base Fluid H_2O	$Al_2O_3 + Cu$
$\rho\left(\frac{kg}{m^3}\right)$	997	~1050
$c_p\left(\frac{J}{kgK}\right)$	4180	~3900
$K\left(\frac{W}{mK}\right)$	0.613	~0.75
$\mu\left(\frac{kg}{mS}\right)$	0.001003	~0.0011
$\sigma\left(\frac{S}{m}\right)$	0.05	~0.06

3.0 SOLUTION PROCEDURE

3.1 Analytical Solution

Solving the governing equations (11), (12) and (13) analytically, is challenging task due to the coupled and nonlinear nature shown above. It is good to reduce the present governing equations to a form whose solutions can be obtained and a situation that exhibits an exact solution is the problem of steady-state flow of nanofluid past Riga plate (Ahmad *et al.*, 2016).

3.1.1 Steady-State Solution

This can be obtained by setting $\frac{\partial u}{\partial t} = \frac{\partial \theta}{\partial t} = \frac{\partial \phi}{\partial t} = 0$ into equations (11), (12) and (13) which can be written as:

$$v_w \frac{\partial u}{\partial y} = \frac{\partial^2 u}{\partial y^2} + \lambda\theta - Nr\phi + Ze^{-y} \quad (21)$$

$$v_w \frac{\partial \theta}{\partial y} = \frac{1}{Pr}\frac{\partial^2 \theta}{\partial y^2} + Nb\frac{\partial \theta}{\partial y}\frac{\partial \phi}{\partial y} + Nt\left(\frac{\partial \theta}{\partial y}\right)^2 \quad (22)$$

$$v_w \frac{\partial \phi}{\partial y} = \frac{1}{Le}\frac{\partial^2 \phi}{\partial y^2} + \frac{1}{Le}\frac{Nt}{Nb}\frac{\partial^2 \theta}{\partial y^2} \quad (23)$$

Using perturbation method, equation (21) can be solved after developing the solution of θ and ϕ, so we consider equations (22) and (23) are independent of equation (21). And also consider Nt and Nb of $O(\varepsilon), \varepsilon \to 0$, since for nanoparticles the magnitude of thermophoretic and Brownian motion parameters are very small.

Expanding θ and $\emptyset$ in small parameter ε, we have:

$$\theta = \theta_0 + \varepsilon\theta_1 + \varepsilon^2\theta_2 + \cdots \quad (24)$$

$$\phi = \phi_0 + \varepsilon\phi_1 + \varepsilon^2\phi_2 + \cdots \quad (25)$$

And set $Nb = b\varepsilon$ and $Nt = a\varepsilon$, for suction velocity, we set $v_w = -s, s > 0$

3.1.1.1 Zeroth Order Solution

Using equations (24) and (25) into equations (22) and (23), we have:

DOI: https://doi.org/10.57233/ijsgs.v11i2.854 ISSNp: 2488-9229; ISSNe: 3027-1118
IJSGS FUGUSAU VOLXXX WEBSITE: https://fugus-ijsgs.com.ng

$$-s\frac{\partial\theta_0}{\partial y}=\frac{1}{Pr}\frac{\partial^2\theta_0}{\partial y^2} \quad (26)$$

$$-s\frac{\partial\phi_0}{\partial y}=\frac{1}{Le}\frac{\partial^2\emptyset_0}{\partial y^2}+\frac{1}{Le}\frac{a}{b}\frac{\partial^2\theta_0}{\partial y^2} \quad (27)$$

Using boundary condition

$$\left.\begin{array}{lll}\theta_0=1, & \phi_0=1 & at\ y=0\\ \theta_0=0, & \phi_0=0 & as\ y\to\infty\end{array}\right\} \quad (28)$$

The solution obtained is given as:

$$\theta_0(y)=e^{-sPry} \quad (29)$$

$$\emptyset_0(y)=-\frac{aPr(e^{-sLey}-e^{-sPry})+b(Le-Pr)e^{-sLey}}{b(Le-Pr)} \quad (30)$$

3.1.1.2 First Order Solution

Using equations (24) and (25) into equations (22) and (23), we have:

$$-s\frac{\partial\theta_0}{\partial y}=\frac{1}{Pr}\frac{\partial^2\theta_1}{\partial y^2}+b\frac{\partial\theta_0}{\partial y}\frac{\partial\phi_0}{\partial y}+a\left(\frac{\partial\theta_0}{\partial y}\right)^2 \quad (31)$$

$$-s\frac{\partial\phi_1}{\partial y}=\frac{1}{Le}\frac{\partial^2\phi_1}{\partial y^2}+\frac{1}{Le}\frac{Nt}{Nb}\frac{\partial^2\theta_1}{\partial y^2} \quad (32)$$

Using boundary condition

$$\left.\begin{array}{lll}\theta_1=0, & \phi_1=0 & at\ y=0\\ \theta_1=0, & \phi_1=0 & as\ y\to\infty\end{array}\right\} \quad (33)$$

The solution obtained is given as:

$$\theta_1(y)=\frac{aLePr}{2(Le-Pr)}e^{-2sPry}+\frac{2aPr^2+LePr+2bPr^2}{2(Le-Pr)}e^{-sPry}+\frac{aPr^3+bPr^3-bLePr^2}{Le^2-Pr^2}e^{-s(Pr+Le)y} \quad (34)$$

$$\begin{aligned}\phi_1(y)&=\frac{4abLe^2Pr^2+3a^2Le^2Pr^2-2abLe^3Pr}{2b(Le-2Pr)(Le^2-Pr^2)}e^{-sLey}-\frac{a^2Le^2Pr^2+a^2LePr^3}{b(Le-2Pr)(Le^2-Pr^2)}e^{-2sPry}\\&+\frac{a^2Le^2Pr^2-4aPr^4+2abLePr^3-2abPr^4}{2b(Le-2Pr)(Le^2-Pr^2)}e^{-sPry}\\&+\frac{Pra(Le^3b-2bPrLe-aPrLe^2-bPr^2Le+aPr^2Le+2bPr^3+2aPr^3)}{b(Le-2Pr)(Le^2-Pr^2)}e^{-s(Pr+Le)y}\end{aligned} \quad (35)$$

After determining the solutions of θ and ϕ profiles up to $O(\varepsilon^2)$, we use equation (21) to determine the velocity profile with boundary condition in equation 14, consider:

$$u=u_0+\varepsilon u_1+\varepsilon^2u_2\ \cdots \quad (36)$$

The solutions of $O(1)$ and $O(\varepsilon)$ for $Le=2$ and $Pr=7$are obtained as:

$$\begin{aligned}u_0=&\frac{84bs^2(1-s+Z)+2\lambda b(1-s)+14aNr(s-1)+42Nr(a+b)(s-1)}{84(s-1)}e^{-sy}\frac{Ze^{-y}}{s-1}\\&+\frac{5bNr+7aNr}{10bs^2}e^{-2sy}+\frac{7aNr-5b\lambda}{42bs^2}e^{-7sy}\end{aligned} \quad (37)$$

$$\begin{aligned}u_1=&-\frac{49}{40}\left(\frac{5}{51597}(1911abNr-455b^2\lambda+1911a^2Nr-421ab\lambda)-\frac{2}{9}\left(a^2Nr+\frac{8}{7}abNr\right)e^{-sy}\right.\\&+\frac{1}{270}\left(\frac{32}{7}a^2Nr+\frac{160}{49}ab\lambda+4abNr+\frac{20}{7}b^2\lambda\right)e^{-6sy}\\&\left.-\frac{1}{9}\left(\frac{5}{3}abNr+\frac{5}{9}b^2\lambda+a^2Nr+\frac{7}{9}ab\lambda\right)e^{-8sy}+\frac{2}{7}\left(\frac{1}{39}a^2Nr+\frac{2}{91}ab\lambda\right)e^{-13sy}\right)\frac{e^{-sy}}{bs^2}\end{aligned} \quad (38)$$

Considering the following general forms for steady-state solutions

$$\theta_s(y)\approx\theta_0(y)+\varepsilon\theta_1(y) \quad (39)$$

$$\phi_s(y)\approx\phi_0(y)+\varepsilon\phi_1(y) \quad (40)$$

$$u_s(y)\approx u_0(y)+\varepsilon u_1(y) \quad (41)$$

Where $\theta_s(y),\phi_s(y)$ and $u_s(y)$ are steady-state solutions of temperature, nanoparticle concentration and velocity profiles respectively, substituting equations (29), (30), (34), (35), (37), (38) into (39), (40) and (41), we have:

$$\begin{aligned}\theta_s(y)\approx e^{-sPry}+\varepsilon\left(\frac{aLePr}{2(Le-Pr)}e^{-2sPry}+\frac{2aPr^2+LePr+2bPr^2}{2(Le-Pr)}e^{-sPry}\right.\\\left.+\frac{aPr^3+bPr^3-bLePr^2}{Le^2-Pr^2}e^{-s(Pr+Le)y}\right)\end{aligned} \quad (42)$$

DOI: https://doi.org/10.57233/ijsgs.v11i2.854 ISSNp: 2488-9229; ISSNe: 3027-1118

IJSGS FUGUSAU VOLXXX WEBSITE: https://fugus-ijsgs.com.ng

$$\phi_s(y) \approx -\frac{aPr(e^{-sLey}-e^{-sPry})+b(Le-Pr)e^{-sLey}}{b(Le-Pr)} + \varepsilon\left(\frac{4abLe^2Pr^2+3a^2Le^2Pr^2-2abLe^3Pr}{2b(Le-2Pr)(Le^2-Pr^2)}e^{-sLey}-\frac{a^2Le^2Pr^2+a^2LePr^3}{b(Le-2Pr)(Le^2-Pr^2)}e^{-2sPry} + \frac{a^2Le^2Pr^2-4aPr^4+2abLePr^3-2abPr^4}{2b(Le-2Pr)(Le^2-Pr^2)}e^{-sPry} + \frac{Pra(Le^3b-2bPrLe-aPrLe^2-bPr^2Le+aPr^2Le+2bPr^3+2aPr^3)}{b(Le-2Pr)(Le^2-Pr^2)}e^{-s(Pr+Le)y}\right) \quad (43)$$

$$u_s(y) \approx \frac{84bs^2(1-s+Z)+2\lambda b(1-s)+14aNr(s-1)+42Nr(a+b)(s-1)}{84(s-1)}e^{-sy}\frac{Ze^{-y}}{s-1} + \frac{5bNr+7aNr}{10bs^2}e^{-2sy}+\frac{7aNr-5b\lambda}{42bs^2}e^{-7sy} + \varepsilon\left[-\frac{49}{40}\left(\frac{5}{51597}(1911abNr-455b^2\lambda+1911a^2Nr-421ab\lambda) - \frac{2}{9}\left(a^2Nr+\frac{8}{7}abNr\right)e^{-sy}+\frac{1}{270}\left(\frac{32}{7}a^2Nr+\frac{160}{49}ab\lambda+4abNr+\frac{20}{7}b^2\lambda\right)e^{-6sy} - \frac{1}{9}\left(\frac{5}{3}abNr+\frac{5}{9}b^2\lambda+a^2Nr+\frac{7}{9}ab\lambda\right)e^{-8sy} + \frac{2}{7}\left(\frac{1}{39}a^2Nr+\frac{2}{91}ab\lambda\right)e^{-13sy}\right)\frac{e^{-sy}}{bs^2}\right] \quad (44)$$

The Nusselt number Nu and Sherwood number Sh at steady-state are given by:

$$Nu = sPr + \varepsilon\left(\frac{asLePr^2}{(Le-Pr)}+\frac{(2asPr^3+sLePr^2+2bsPr^3)}{2(Le-Pr)} + \frac{(aPr^3+bPr^3-bLePr^2)(Pr+Le)s}{Le^2-Pr^2}\right) \quad (45)$$

$$Sh = -\frac{asPr(Le-Pr)+bsLe(Le-Pr)}{b(Le-Pr)} + \varepsilon\left(\frac{sLe(4abLe^2Pr^2+3a^2Le^2Pr^2-2abLe^3\mathrm{Pr})}{2b(Le-2Pr)(Le^2-Pr^2)}-\frac{2sPr(a^2Le^2Pr^2+a^2LePr^3)}{b(Le-2Pr)(Le^2-Pr^2)} + \frac{sPr(a^2Le^2Pr^2-4aPr^4+2abLePr^3-2abPr^4)}{2b(Le-2Pr)(Le^2-Pr^2)} + \frac{s(Pr+Le)\left(Pra(Le^3b-2bPrLe-aPrLe^2-bPr^2Le+aPr^2Le+2bPr^3+2aPr^3)\right)}{b(Le-2Pr)(Le^2-Pr^2)}\right) \quad (46)$$

The skin friction at steady-state is given by:

$$Sf = \frac{\partial u_s}{\partial y}\Big|_{y=0}$$

$$Sf = \frac{\left(84bs^2(1-s+Z)+2\lambda b(1-s)+14aNr(s-1)+42Nr(a+b)(s-1)\right)}{84(1-s)}\frac{Z(s+1)}{s-1}-\frac{5bNr+7aNr}{5bs} - \frac{(7aNr-5b\lambda)}{6bs} + \varepsilon\left[\frac{49}{40}\left(\frac{5}{51597}(1911abNr-455b^2\lambda+1911a^2Nr-421ab\lambda)+\frac{2}{9}s\left(a^2Nr+\frac{8}{7}abNr\right) - \frac{6s}{270}\left(\frac{32}{7}a^2Nr+\frac{160}{49}ab\lambda+4abNr+\frac{20}{7}b^2\lambda\right)+\frac{8s}{9}\left(\frac{5}{3}abNr+\frac{5}{9}b^2\lambda+a^2Nr+\frac{7}{9}ab\lambda\right) - \frac{26s}{7}\left(\frac{1}{39}a^2Nr+\frac{2}{91}ab\lambda\right)\right)\frac{1}{bs}\right] \quad (47)$$

3.1.2 Transient- State Solution

We consider small perturbations and use Laplace transforms to solve the transient governing equations (11), (12) and (13) with boundary conditions equation (14) and initial conditions

$$u(y,0)=0, \quad \theta(y,0)=0, \quad \phi(y,0)=0 \quad as\ t\to 0$$

DOI: https://doi.org/10.57233/ijsgs.v11i2.854 ISSNp: 2488-9229; ISSNe: 3027-1118
IJSGS FUGUSAU VOLXXX WEBSITE: https://fugus-ijsgs.com.ng

Assuming small perturbations and neglecting nonlinear terms and constant suction velocity ($v_w = -s, s > 0$) and applying

$$\mathcal{L}\{f(y,t)\} = \tilde{f}(y,s) = \int_0^\infty e^{-st} f(y,t)dt \qquad (48)$$

Into the governing equations (11), (12) and (13). We obtained the reduced ODEs:

$$s\tilde{u} - u(y,0) - s\frac{d\tilde{u}}{dy} = \frac{d^2\tilde{u}}{dy^2} + \lambda\tilde{\theta} - Nr\tilde{\phi} + \frac{Ze^{-y}}{s} \qquad (49)$$

$$s\tilde{\theta} - \theta(y,0) - s\frac{d\tilde{\theta}}{dy} = \frac{1}{Pr}\frac{d^2\tilde{\theta}}{dy^2} \qquad (50)$$

$$s\tilde{\phi} - \emptyset(y,0) - s\frac{d\tilde{\phi}}{dy} = \frac{1}{Le}\frac{d^2\tilde{\phi}}{dy^2} + \frac{1}{Le}\frac{Nt}{Nb}\frac{d^2\tilde{\theta}}{dy^2} \qquad (51)$$

From equation (14), $\theta(y,0) = 0$, substituting into equation (50), we obtained:

$$\frac{d^2\tilde{\theta}}{dy^2} + sPr\frac{d\tilde{\theta}}{dy} - sPr\tilde{\theta} = 0 \qquad (52)$$

Characteristic equation of equation $m^2 + sPrm - sPr = 0$ give roots:

$$m_{1,2} = \frac{-sPr \pm \sqrt{(sPr)^2 + 4sPr}}{2}$$

Applying equation (14), the physical viability solution (decaying as $y \to \infty$) is:

$$\tilde{\theta}(y,s) = \frac{1}{s}e^{m_1 y} \qquad (53)$$

Where $m_1 = \frac{-sPr-\sqrt{(sPr)^2+4sPr}}{2}$

The transient component $\theta_t(y,t)$ is obtained by inverse Laplace Transform focusing on the dominant pole at $s = -\frac{4}{Pr}$ yielding:

$$\theta_t(y,t) \approx C_{10}e^{-\frac{4}{Pr}t}e^{-\alpha y} \qquad (54)$$

Also from equation (14), $\phi(y,0) = 0$, substituting into equation (51), we obtained:

$$\frac{1}{Le}\frac{d^2\tilde{\phi}}{dy^2} + s\frac{d\tilde{\phi}}{dy} - s\tilde{\phi} = -\frac{1}{Le}\frac{Nt}{Nb}\frac{d^2\tilde{\theta}}{dy^2} \qquad (55)$$

Solving equation (59), we obtained:

$$\tilde{\phi}(y,s) = \frac{1}{s}e^{m_3 y} + C_5 e^{m_4 y} \qquad (56)$$

The transient component $\phi_t(y,t)$ is derived by evaluating residues, with dominant pole at $s = -\frac{4}{Le}$:

$$\phi_t(y,t) \approx C_{11}e^{-\frac{4}{Le}t}e^{-\beta y} \qquad (57)$$

And from equation (14), $u(y,0) = 0$, substituting into equation (49), we obtained:

$$s\tilde{u} - s\frac{d\tilde{u}}{dy} = \frac{d^2\tilde{u}}{dy^2} + s\frac{d\tilde{u}}{dy} - s\tilde{u} = -\lambda\tilde{\theta} + Nr\tilde{\phi} - \frac{Ze^{-y}}{s} \qquad (58)$$

Solving equation (58), we get:

$$\tilde{u}(y,s) = \frac{1}{s}e^{m_5 y} + C_7 e^{-y} + C_8 e^{m_5 y} + C_9 e^{m_6 y} \qquad (59)$$

Where $m_{5,6} = \frac{-s\pm\sqrt{s^2+4s}}{2}, C_7 = \frac{Z}{(m_5^2+sm_5-s)s}, C_8 = \frac{\lambda - NrC_5}{(m_5^2+sm_5-s)s}, C_9 = \frac{Nr}{(m_5^2+sm_5-s)s}$

The transient component $u_t(y,t)$ is obtained by focusing on dominant pole at $s = -4$:

$$u_t(y,t) \approx C_{12}e^{-4t}e^{-\gamma y} \qquad (60)$$

The transient velocity $u(y,t)$, temperature $\theta(y,t)$ and nanoparticle concentration $\emptyset(y,t)$ profiles are given in the forms:

$$\left.\begin{aligned} u(y,t) &\approx u_s(y,t) + u_t(y,t) \\ \theta(y,t) &\approx \theta_s(y,t) + \theta_t(y,t) \\ \phi(y,t) &\approx \phi_s(y,t) + \phi_t(y,t) \end{aligned}\right\} \qquad (61)$$

Where $u_s(y,t), \theta_s(y,t)$ and $\phi_s(y,t)$ are steady-state velocity, temperature and nanoparticle concentration profiles and $u_t(y,t), \theta_t(y,t)$ and $\phi_t(y,t)$ are transient components of velocity, temperature and nanoparticle concentration respectively.

Thus;

DOI: https://doi.org/10.57233/ijsgs.v11i2.854 ISSNp: 2488-9229; ISSNe: 3027-1118

IJSGS FUGUSAU VOLXXX WEBSITE: https://fugus-ijsgs.com.ng

$$u(y,t) \approx \frac{84bs^2(1-s+Z)+2\lambda b(1-s)+14aNr(s-1)+42Nr(a+b)(s-1)}{84(s-1)}e^{-sy}\frac{Ze^{-y}}{s-1} + \frac{5bNr+7aNr}{10bs^2}e^{-2sy} + \frac{7aNr-5b\lambda}{42bs^2}e^{-7sy} + \varepsilon\left[-\frac{49}{40}\left(\frac{5}{51597}(1911abNr-455b^2\lambda+1911a^2Nr-421ab\lambda) - \frac{2}{9}\left(a^2Nr+\frac{8}{7}abNr\right)e^{-sy} + \frac{1}{270}\left(\frac{32}{7}a^2Nr+\frac{160}{49}ab\lambda+4abNr+\frac{20}{7}b^2\lambda\right)e^{-6sy} - \frac{1}{9}\left(\frac{5}{3}abNr+\frac{5}{9}b^2\lambda+a^2Nr+\frac{7}{9}ab\lambda\right)e^{-8sy} + \frac{2}{7}\left(\frac{1}{39}a^2Nr+\frac{2}{91}ab\lambda\right)e^{-13sy}\right)\frac{e^{-sy}}{bs^2}\right] + C_{12}e^{-4t}e^{-\gamma y} \quad (62)$$

$$\theta(y,t) \approx e^{-sPry} + \varepsilon\left(\frac{aLePr}{2(Le-Pr)}e^{-2sPry} + \frac{2aPr^2+LePr+2bPr^2}{2(Le-Pr)}e^{-sPry} + \frac{aPr^3+bPr^3-bLePr^2}{Le^2-Pr^2}e^{-s(Pr+Le)y}\right) + C_{10}e^{-\frac{4}{Pr}t}e^{-\alpha y} \quad (63)$$

$$\phi(y,t) \approx -\frac{aPr(e^{-sLey}-e^{-sPry})+b(Le-Pr)e^{-sLey}}{b(Le-Pr)} + \varepsilon\left(\frac{4abLe^2Pr^2+3a^2Le^2Pr^2-2abLe^3Pr}{2b(Le-2Pr)(Le^2-Pr^2)}e^{-sLey} - \frac{a^2Le^2Pr^2+a^2LePr^3}{b(Le-2Pr)(Le^2-Pr^2)}e^{-2sPry} + \frac{a^2Le^2Pr^2-4aPr^4+2abLePr^3-2abPr^4}{2b(Le-2Pr)(Le^2-Pr^2)}e^{-sPry} + \frac{Pra(Le^3b-2bPrLe-aPrLe^2-bPr^2Le+aPr^2Le+2bPr^3+2aPr^3)}{b(Le-2Pr)(Le^2-Pr^2)}e^{-s(Pr+Le)y}\right) + C_{11}e^{-\frac{4}{Le}t}e^{-\beta y} \quad (64)$$

3.2 Numerical Solution

The governing equations (11)-(13) are solved using an explicit finite difference method (EFDM). The spatial domain $y \in [0,1]$ is discretized into N uniformly spaced nodes with grid spacing $\Delta y = \frac{1}{N-1}$. And time is advanced with step size Δt. The variables u, θ and $\emptyset$ at grid point i and time step n are denoted by u_i^n, θ_i^n and $\emptyset_i^n$.

Using forward difference in time and central difference in space for equation (11), we get

$$\frac{u_i^{n+1}-u_i^n}{\Delta t} + (v_w)_i^n\left(\frac{u_{i+1}^n-u_{i-1}^n}{2\Delta y}\right) = \frac{u_{i+1}^n-2u_i^n+u_{i-1}^n}{(\Delta y)^2} + \lambda\theta_i^n - Nr\phi_i^n + Ze^{-y_i} \quad (65)$$

Rearranging for u_i^{n+1}, we get

$$u_i^{n+1} = u_i^n + \Delta t\left(\frac{u_{i+1}^n-2u_i^n+u_{i-1}^n}{(\Delta y)^2} + s\left(\frac{u_{i+1}^n-u_{i-1}^n}{2\Delta y}\right) + \lambda\theta_i^n - Nr\phi_i^n + Ze^{-y_i}\right) \quad (66)$$

Using forward difference in time and central difference in space for equation (12), we get

$$\frac{\theta_i^{n+1}-\theta_i^n}{\Delta t} + (v_w)_i^n\left(\frac{\theta_{i+1}^n-\theta_{i-1}^n}{2\Delta y}\right) = \frac{1}{Pr}\frac{\theta_{i+1}^n-2\theta_i^n+\theta_{i-1}^n}{(\Delta y)^2} + Nb\frac{\phi_{i+1}^n-\phi_{i-1}^n}{2\Delta y}\frac{\theta_{i+1}^n-\theta_{i-1}^n}{2\Delta y} + Nt\left(\frac{\theta_{i+1}^n-\theta_{i-1}^n}{2\Delta y}\right)^2 \quad (67)$$

Rearranging for θ_i^{n+1}, we obtain

$$\theta_i^{n+1} = \theta_i^n + \Delta t\left[\frac{1}{Pr}\frac{\theta_{i+1}^n-2\theta_i^n+\theta_{i-1}^n}{(\Delta y)^2} + s\left(\frac{\theta_{i+1}^n-\theta_{i-1}^n}{2\Delta y}\right) + Nb\frac{\phi_{i+1}^n-\phi_{i-1}^n}{2\Delta y}\frac{\theta_{i+1}^n-\theta_{i-1}^n}{2\Delta y} + Nt\left(\frac{\theta_{i+1}^n-\theta_{i-1}^n}{2\Delta y}\right)^2\right] \quad (68)$$

Using forward difference in time and central difference in space for equation (13), we get

$$\frac{\phi_i^{n+1}-\phi_i^n}{\Delta t} + (v_w)_i^n\left(\frac{\phi_{i+1}^n-\phi_{i-1}^n}{2\Delta y}\right) = \frac{1}{Le}\frac{\phi_{i+1}^n-2\phi_i^n+\phi_{i-1}^n}{(\Delta y)^2} + \frac{1}{Le}\frac{Nt}{Nb}\frac{\theta_{i+1}^n-2\theta_i^n+\theta_{i-1}^n}{(\Delta y)^2} \quad (69)$$

Rearranging for ϕ_i^{n+1}, we get

$$\phi_i^{n+1} = \phi_i^n + \Delta t\left(\frac{1}{Le}\frac{\phi_{i+1}^n-2\phi_i^n+\phi_{i-1}^n}{(\Delta y)^2} + \frac{1}{Le}\frac{Nt}{Nb}\frac{\theta_{i+1}^n-2\theta_i^n+\theta_{i-1}^n}{(\Delta y)^2} - (v_w)_{i,j}^n\left(\frac{\phi_{i+1}^n-\phi_{i-1}^n}{2\Delta y}\right)\right) \quad (70)$$

DOI: https://doi.org/10.57233/ijsgs.v11i2.854 ISSNp: 2488-9229; ISSNe: 3027-1118
IJSGS FUGUSAU VOLXXX WEBSITE: https://fugus-ijsgs.com.ng

Subjected to fixed (time independent) boundary conditions

$$\left.\begin{array}{lll} U_0^n = 0, & \phi_0^n = -1, & \theta_0^n = -1 \\ U_N^n = 0, & \phi_N^n = 1, & \theta_N^n = 1 \end{array}\right\} \quad (71)$$

Equations (82), (84) and (86) are momentum, energy and concentration equations respectively. And the above equations are then solved using the Thomas algorithm which includes the transformation into a system of linear algebraic equations in the tridiagonal form.

The solution to the equations was obtained by numerical integration. In each time step, the solution to the volumetric fraction of nanoparticles is first obtained. This is then used to get the temperature θ after which the velocity u is obtained by using already known values of θ and ϕ. The computation is continued until steady-state is achieved that satisfies the following convergence criteria condition:

$$max\left(\frac{|u^{n+1}-u^n|}{|u^n|}, \quad \frac{|\theta^{n+1}-\theta^n|}{|\theta^n|}, \quad \frac{|\phi^{n+1}-\phi^n|}{|\phi^n|}\right) < 10^{-6} \quad (72)$$

where $u_i^{n+1}, \theta_i^{n+1}, \phi_i^{n+1}$ stands for velocity, temperature fields and nanoparticle volume fraction. The residual based is

$$\left|\left|\frac{\partial u}{\partial t}\right|\right| + \left|\left|\frac{\partial \theta}{\partial t}\right|\right| + \left|\left|\frac{\partial \phi}{\partial t}\right|\right| < \varepsilon \quad (73)$$

With relative error of

$$\left(\frac{|u^{n+1}-u^n|}{|u^n|}, \quad \frac{|\theta^{n+1}-\theta^n|}{|\theta^n|}, \quad \frac{|\phi^{n+1}-\phi^n|}{|\phi^n|}\right) < 10^{-6} \quad (74)$$

To ascertain the correctness of the numerical procedure used, the results of this present approach are compared with that of the analytical solution obtained for the steady-state. This gives credibility to the accuracy of the numerical solution in obtaining the solution to the problem.

3.3 Entropy Generation Analysis

For hybrid nanofluids over Riga plate, the entropy analysis is given by:

$$S''_{gen} = \frac{k_{hnf}}{T_\infty^2}(\nabla T)^2 + \frac{\mu_{hnf}}{T_\infty}\left(\frac{\partial u}{\partial y}\right)^2 + \frac{\sigma_{hnf}B_0}{T_\infty}u^2 + \frac{RD_B}{C_\infty}(\nabla C)^2 + \frac{RD_T}{T_\infty}(\nabla T \cdot \nabla C) \quad (75)$$

Where $k_{hnf}, \mu_{hnf}, \sigma_{hnf}, B_0$ and R are hybrid nanofluid thermal conductivity, dynamic viscosity, electrical conductivity, magnetic field strength and gas constant respectively.
Introducing the dimensionless entropy generation number N_s into equation (75), where

$$N_s = \frac{S''_{gen}}{S_0} \text{ and } S_0 = \frac{k_{hnf}\Delta T^2}{L^2 T_\infty^2}$$

Results to:

$$N_s = \left(\frac{\partial \theta}{\partial y}\right)^2 + \frac{Br}{\Omega}\left(\frac{\partial u}{\partial y}\right)^2 + \frac{BrZ}{\Omega}u^2 + \frac{\Gamma}{Le}\left(\frac{\partial \emptyset}{\partial y}\right)^2 + \Gamma\frac{Nt}{Nb}\left(\frac{\partial \theta}{\partial y}\frac{\partial \emptyset}{\partial y}\right) \quad (76)$$

Where Br, Ω and Γ are Brinkman number, temperature difference ratio and diffusion ratio respectively.

3.4 Bejan Number Analysis

For hybrid nanofluid over Riga plate, Bejan number is given by:

$$Be(y,t) = \frac{\left(\frac{\partial \theta}{\partial y}\right)^2}{N_s} \quad (77)$$

3.5 Stability Analysis

By Ansatz perturbation, the perturbed components are:

$$u(y,t) = u_s(y) + \hat{u}(y)e^{\sigma t}, \quad \theta(y,t) = \theta_s(y) + \hat{\theta}(y)e^{\sigma t}, \quad \phi(y,t) = \phi_s(y) + \hat{\phi}(y)e^{\sigma t} \quad (78)$$

where u_s, θ_s, ϕ_s are steady-state solutions and $\hat{u}$, $\hat{\theta}$, $\hat{\phi}$ are infinitesimal perturbations and $\sigma = \sigma_T + i\sigma_i$ is growth rate. By substituting into equations (11)-(13) and neglecting higher-order terms, we have:

$$\sigma\hat{u} + v_w\frac{\partial \hat{u}}{\partial y} = \frac{\partial^2 \hat{u}}{\partial y^2} + \lambda\hat{\theta} - Nr\hat{\phi} \quad (79)$$

$$\sigma\hat{\theta} + v_w\frac{\partial \hat{\theta}}{\partial y} = \frac{1}{Pr}\frac{\partial^2 \hat{\theta}}{\partial y^2} + Nb\left(\frac{\partial \theta_s}{\partial y}\frac{\partial \hat{\phi}}{\partial y} + \frac{\partial \phi_s}{\partial y}\frac{\partial \hat{\theta}}{\partial y}\right) + 2Nt\frac{\partial \theta_s}{\partial y}\frac{\partial \hat{\theta}}{\partial y} \quad (80)$$

DOI: https://doi.org/10.57233/ijsgs.v11i2.854 ISSNp: 2488-9229; ISSNe: 3027-1118
IJSGS FUGUSAU VOLXXX WEBSITE: https://fugus-ijsgs.com.ng

$$\sigma\hat{\phi} + v_w \frac{\partial \hat{\phi}}{\partial y} = \frac{1}{Le}\frac{\partial^2 \hat{\phi}}{\partial y^2} + \frac{1}{Le}\frac{Nt}{Nb}\frac{\partial^2 \hat{\theta}}{\partial y^2} \quad (81)$$

Subjected to boundary conditions

$$\hat{u}(0) = \hat{\theta}(0) = \hat{\phi}(0) = 0, \qquad \hat{u}(\infty) = \hat{\theta}(\infty) = \hat{\phi}(\infty) = 0 \quad (82)$$

Assuming normal mode solutions for perturbations for eigenvalue analysis:

$$\hat{u}(y) = U_0(y)e^{\sigma t}, \qquad \hat{\theta}(0) = \Theta_0(y)e^{\sigma t}, \qquad \hat{\phi}(0) = \Phi_0(y)e^{\sigma t} \quad (83)$$

Substituting into equations (79)-(81) and approximating the system using constant coefficients, we have;

$$(\sigma + sk - k^2)U_0 + \lambda\Theta_0 - Nr\Phi_0 = 0 \quad (84)$$

$$\left(\sigma + sk - \frac{k^2}{Pr} - Nbs^2 PrLe - 2Nts^2\mathrm{Pr}\right)\Theta_0 = 0 \quad (85)$$

$$\left(\sigma + sk - \frac{k^2}{Le}\right)\Phi_0 + \frac{Nt}{NbLe}k^2\Theta_0 = 0 \quad (86)$$

Where $\theta_s' \approx -sPre^{-sPry}$, $\emptyset_s' \approx -sLee^{-sLey}$ for steady-state. Combining equations (84)-(86) into a matrix form:

$$\begin{pmatrix} \sigma + sk - k^2 & \lambda & -Nr \\ 0 & \sigma + sk - \frac{k^2}{Pr} - Nbs^2 PrLe - 2Nts^2\mathrm{Pr} & 0 \\ 0 & \frac{Nt}{NbLe}k^2 & \sigma + sk - \frac{k^2}{Le} \end{pmatrix}\begin{pmatrix} U_0 \\ \Theta_0 \\ \Phi_0 \end{pmatrix} = \begin{pmatrix} 0 \\ 0 \\ 0 \end{pmatrix} \quad (87)$$

The simplified determinant is given by:

$$(\sigma + sk - k^2)\left(\sigma + sk - \frac{k^2}{Pr} - \beta\right)\left(\sigma + sk - \frac{k^2}{Le}\right) = 0 \quad (88)$$

For $\beta = Nbs^2 PrLe + 2Nts^2\mathrm{Pr}$, yielding three roots for σ, momentum mode $(\sigma = k^2 - sk)$, thermal mode $\left(\sigma = \frac{k^2}{Pr} - sk + \beta\right)$ and concentration mode $\left(\sigma = \frac{k^2}{Le} - sk\right)$

Momentum mode is stable if $k < s$, thermal mode is stable if $\frac{k^2}{Pr} + \beta < sk$, and concentration mode is stable if $\frac{k^2}{Le} < sk$. The critical parameter $\beta > 0$ for dominant thermal mode $k = sPr$ resulting to thermal mode instability unless suction (s) is large enough to dominate. The system is conditionally stable, with stability controlled by suction strength and EMHD effects.

4.0 RESULTS AND DISCUSSION

Figure 1 above presents a schematic diagram of the Riga plate, which consists of an alternating array of electrodes and permanent magnets. This setup is crucial for generating the Lorentz force that manipulates the boundary layer flow, forming the basis for the study's theoretical and numerical analysis.

Figures 2 and 3 depict the steady-state velocity and temperature profiles, respectively, under varying parameters. Figure 2 shows how the modified Hartmann number Z influences the velocity profile, highlighting the EMHD effects on fluid motion. Figure 3 demonstrates the impact of the Prandtl number Pr on the temperature distribution, emphasizing the role of thermal diffusivity in heat transfer. These figures reveal that increasing Z enhances the velocity profile, while higher Pr values lead to a steeper temperature gradient near the plate, indicating improved thermal boundary layer control.

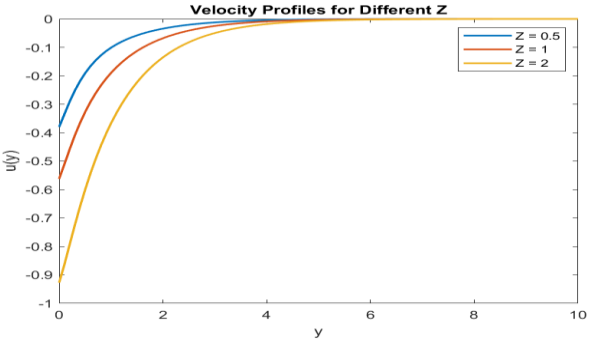

Figure 2: Velocity Profile for Variatons Z

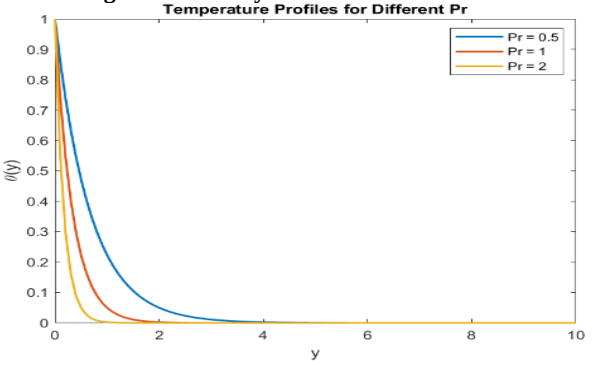

Figure 3: Steady-State Temperature Profile for Different Pr

DOI: https://doi.org/10.57233/ijsgs.v11i2.854 ISSNp: 2488-9229; ISSNe: 3027-1118

The entropy generation analysis is illustrated in Figures 4 and 5. Figure 4 breaks down the contributions of different irreversibility mechanisms, such as viscous dissipation, Joule heating, and thermal gradients, to the total entropy production. Figure 5 further explores the irreversibility ratio, showing how these mechanisms compete or dominate under varying conditions. These results are critical for optimizing energy efficiency in thermal systems. Figure 6 complements this analysis by presenting the Bejan number profile, which quantifies the dominance of heat transfer irreversibility over other forms. The trends suggest that thermal irreversibility is more pronounced near the plate, while viscous effects become significant farther away.

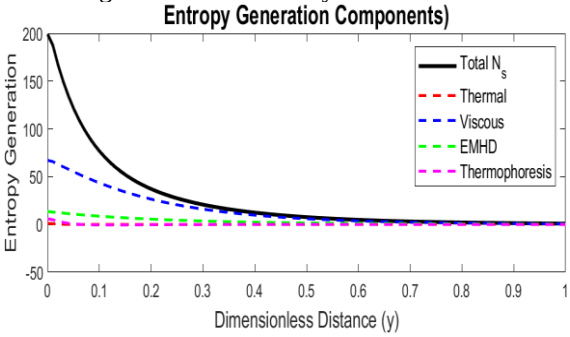

Figure 4: Entropy Generation Components

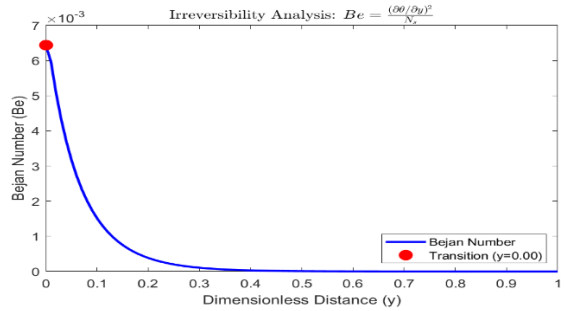

Figure 5: Irreversibility Analysis

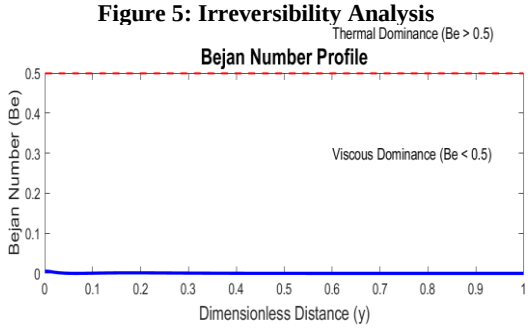

Figure 6: Bejan Number Profile

Transient behavior is captured in Figures 7–9, which display the evolution of velocity, temperature, and nanoparticle concentration profiles over time. These figures highlight the dynamic response of the system to perturbations, with the profiles gradually approaching steady-state conditions. The transient analysis underscores the importance of time-dependent effects in real-world applications, such as microfluidic devices or nuclear cooling systems.

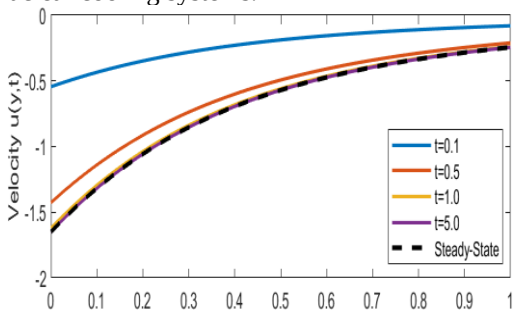

Figure 7: Transient Velocity Profile for Different τ Values

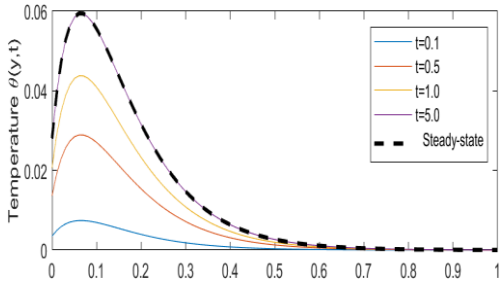

Figure 8: Transient Temperature Profile for Different τ Values

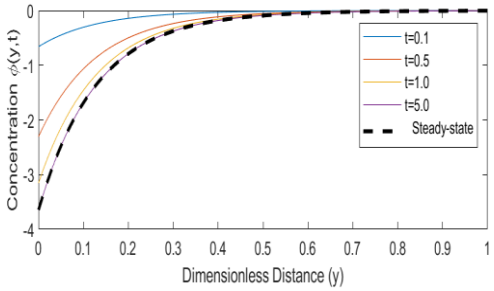

Figure 9: Transient Concentration Profile for Different τ Values

Stability analysis is presented in Figures 10 and 11, where Figure 10 examines the influence of Z on the system's linear stability, and Figure 11 plots the growth rate against the suction parameter s. These figures reveal that stability is highly dependent on EMHD effects and suction strength, with larger s values promoting stability by suppressing perturbations.

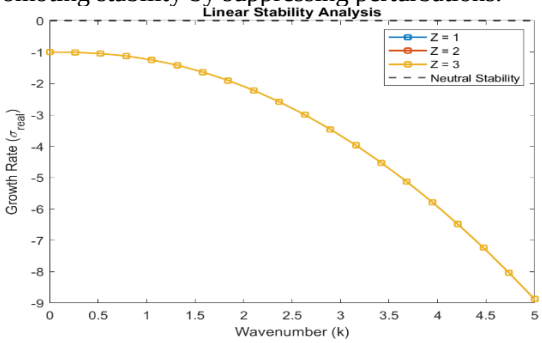

Figure 10: Linear Stability Analysis for Different Values of Z

DOI: https://doi.org/10.57233/ijsgs.v11i2.854 ISSNp: 2488-9229; ISSNe: 3027-1118
IJSGS FUGUSAU VOLXXX WEBSITE: https://fugus-ijsgs.com.ng

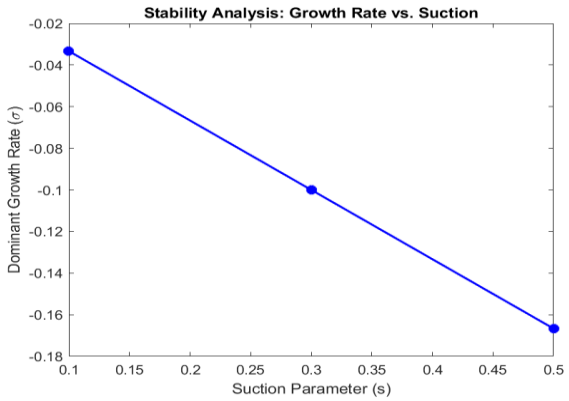

Figure 11: Linear Analysis for Growth Rate Against Suction Parameter *s*

Figures 12–14 compare steady-state and transient profiles, validating the numerical solutions and demonstrating the convergence of transient states to steady-state conditions.

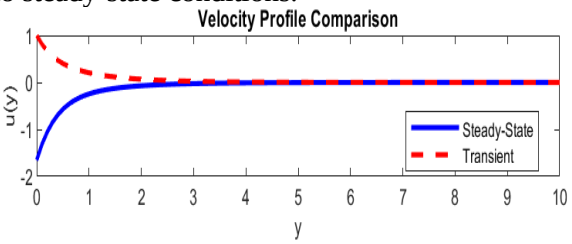

Figure 12: Comparison of Steady-State and Transient State Velocity Profiles

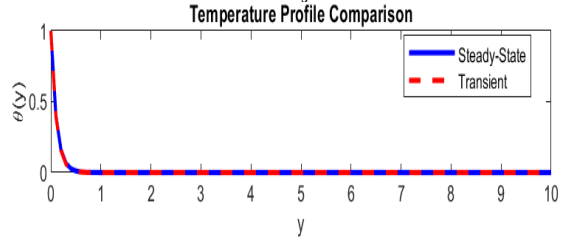

Figure 13: Comparison of Steady-State and Transient State Temperature Profiles

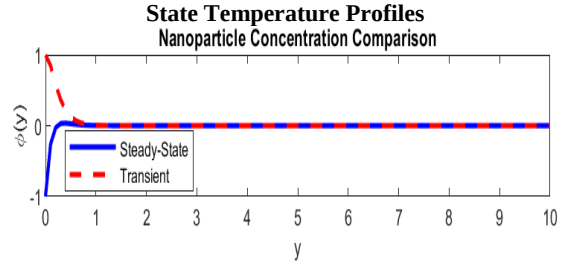

Figure 14: Comparison of Steady-State and Transient State Nanoparticle Concentration Profiles

Finally, Figures 15 and 16 explore the effects of Z and s on the Nusselt and Sherwood numbers, respectively, which are key indicators of heat and mass transfer performance. The results indicate that both parameters significantly enhance heat and mass transfer rates, with practical implications for industrial applications. Figures 18 and 19 further illustrate the evolution of perturbations and their impact on velocity profiles, reinforcing the conditional stability of the system.

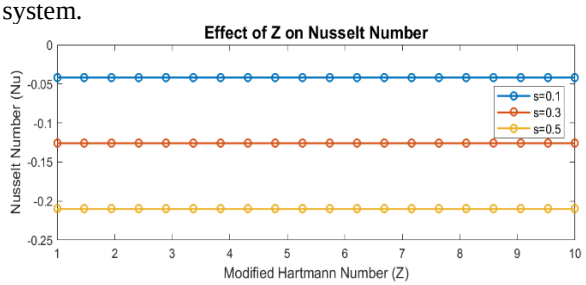

Figure 15: Effect of Nusselt Number Z for Different Values of s

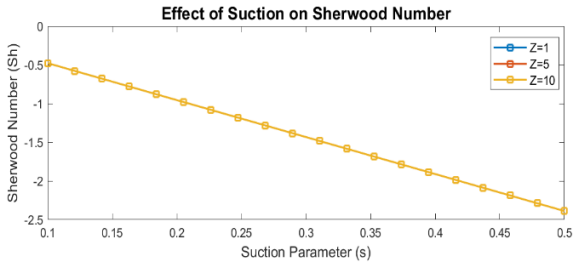

Figure 16: Effect of Suction Parameter s on Sherwood Number Sh for Different Values of Z

5.0 CONCLUSION

This study investigated the transient Electro-Magneto Hydrodynamic (EMHD) control of hybrid nanofluid flow over a two-dimensional Riga plate, with a focus on entropy generation minimization and hydrodynamic stability analysis. The research combined analytical and numerical approaches to explore the complex interplay between electromagnetic forces, nanoparticle interactions, and transient flow dynamics. Key findings include:

The modified Hartmann number Z significantly enhances the velocity profile due to Lorentz force effects, while the Prandtl number Pr influences thermal boundary layer development, with higher Pr values leading to steeper temperature gradients near the plate. The analysis revealed that thermal irreversibility dominates near the plate, while viscous dissipation and Joule heating contribute significantly farther away. Minimizing entropy generation is crucial for optimizing energy efficiency in thermal systems. The transient profiles of velocity, temperature, and nanoparticle concentration demonstrated how the system evolves toward steady-state conditions, emphasizing the importance of time-dependent effects in practical applications. The linear stability study confirmed that the system is conditionally stable, with suction strength (s) and EMHD effects playing a critical role in suppressing perturbations and maintaining flow stability. The Nusselt and Sherwood numbers were found to increase with higher Z and s, indicating improved heat and mass transfer performance, which is beneficial for

applications in microfluidics, nuclear cooling, and aerospace propulsion.

REFERENCES

Ahmad, A., Asghar, S., & Afzal, S. (2016). Flow of nanofluid past a Riga plate. Journal of Magnetism and Magnetic Materials, 402, 44–48. https://doi.org/10.1016/j.jmmm.2015.11.043

Ali, A., Ahmed, M., & Nawaz, R. (2023). Enhanced heat transfer analysis of hybrid nanofluid over a Riga plate: Incorporating Lorentz forces and entropy generation. Tribology International, 88, 108844. https://doi.org/10.1016/j.jmmm.2015.11.043

Bejan, A. (1996). Entropy generation minimization: The new thermodynamics of finite-size devices and finite-time processes. Journal of Applied Physics, 79(3), 1191–1218. https://doi.org/10.1063/1.362674

Choi, S. U. S., & Eastman, J. A. (1995). Enhancing thermal conductivity of fluids with nanoparticles (Report No. ANL/MSD/CP-84938). Argonne National Laboratory.

Dakin-Gari, A. U., Sarki, N. M., Hamza, M. M., Dakin-Gari, S. M. and Yale, I. D. (2024). Free Convective MHD Flow of Jeffrey Fluid in a Porous Medium in the Presence of Heat Source/Sink. International Journal of Science and Global Sustainability, 10(1). DOI: https://doi.org/10.57233/ijsgs.v10i1.600

Gailitis, A., & Lielausis, O. (1961). On a possibility to reduce the hydrodynamic resistance of a plate in an electrolyte. Applied Magnetohydrodynamics, 12, 143–146.

Godwin, O., Emmanuel, O., Hamza, M. M., Onwubuya, I. O. and Abdulsalam, S. (2023). A Computational Analysis on Steady MHD Casson Fluid Flow across A Vertical Porous Channel Affected By Thermal Radiation Effect. International Journal of Science and Global Sustainability, 9(1). https://doi.org/10.57233/ijsgs.v9i1.393

Hamza, M. M., Alao, F. I., & Pop, I. (2022). Effects of Magnetohydrodynamics on time-dependent mixed convection flow of an exothermic fluid in a vertical channel. International Communications in Heat and Mass Transfer, 130, 105785. https://doi.org/10.1016/j.icheatmasstransfer.2021.105785

Hussanan, A., Salleh, M. Z., Khan, I., & Tahar, R. M. (2021). MHD flow and heat transfer of hybrid nanofluids over a stretching sheet: A numerical study. Journal of King Saud University - Engineering Sciences, 33(3), 201–210.

Khatun, S., Islam, M. M., Mollah, M. T., Poddar, S., & Alam, M. M. (2021). EMHD radiating fluid flow along a vertical Riga plate with suction in a rotating system. Springer Nature Applied Sciences, 3(4), 452. https://doi.org/10.1007/s42452-021-04444-4

Mahian, O., Kolsi, L., Amani, M., Estellé, P., Ahmadi, G., Kleinstreuer, C., Marshall, J. S., Siavashi, M., Taylor, R. A., Niazmand, H., Wongwises, S., Hayat, T., Kolanjiyil, A., Kasaeian, A., & Pop, I. (2019). Recent advances in modeling and simulation of nanofluid flows—Part I: Fundamentals and theory. Physics Reports, 790, 1–48. https://doi.org/10.1016/j.physrep.2018.11.004

Moyi, A. U. and Sani, A. (2024). MHD Inclination on Unsteady Basic Gaseous Micro-Flow Past on Sinusoidally Moving Horizontal Plate. International Journal of Science and Global Sustainability, 10(3). DOI: https://doi.org/10.57233/ijsgs.v10i3.695

Muhammad, N. S., Abubakar, I. and Yale I. D. (2024). Unsteady Magnetohydrodynamic (MHD) Free Convective Isothermal Vertical Plate in A Porous Medium with Radiation Effect. International Journal of Science and Global Sustainability, 10(1). DOI: https://doi.org/10.57233/ijsgs.v10i1.590

Saleh, S., Halliru, A., Sarki, N. M. and Emmanuel, O. (2023). Magnetohydrodynamic (MHD) Convective Flow in a Porous Medium in the Presence Variable Pressure and Injection/Suction. International Journal of Science and Global Sustainability, 9(3). https://doi.org/10.57233/ijsgs.v9i3.535

Saleh, S., Saad, N. and Emmanuel, O. (2024). Magnetohydrodynamic (MHD) Convective Flow through a Porous Medium with Magnetic and Chemical Reaction Characteristics. International Journal of Science and Global Sustainability, 10(1). DOI: https://doi.org/10.57233/ijsgs.v10i1.591

Sheikholeslami, M., Jafaryar, M., & Shafee, A. (2022). Transient MHD nanofluid flow in energy systems with Lorentz forces and variable thermal conductivity. International Journal of Heat and Mass Transfer, 182, 121990. https://doi.org/10.1016/j.ijheatmasstransfer.2021.121990

Usman, H. ., Muhammad, A. ., & Omokhuale , E. (2024). Enhancing Thermophoresis Effect on Time-Dependent Magnetohydrodynamics (MHD) Oscillatory Boundary Layer Flow Occupied with Nanoparticles. International Journal of Science for Global Sustainability, 10(1), 197–207. https://doi.org/10.57233/ijsgs.v10i1.611